Stretchable Printed Circuit Board Based on Leak-Free Liquid Metal Interconnection and Local Strain Control

Min Seong Kim, Seunghwan Kim, Jungrak Choi, Seonggi Kim, Chankyu Han, Yung Lee, Youngdo Jung, Jaeho Park, Sunjong Oh, Byeong-Soo Bae, Hyuneui Lim,* and Inkyu Park*

Read Online

ACCESS | Metrics & More | Article Recommendations | Supporting Information

ABSTRACT: In order to realize a transition from conventional to stretchable electronics, it is necessary to make a universal stretchable circuit board in which passive/active components can be robustly integrated. We developed a stretchable printed circuit board (s-PCB) platform that enables easy and reliable integration of various electronic components by utilizing a modulus-gradient polymeric substrate, liquid metal amalgam (LMA) circuit traces, and Ag nanowire (AgNW) contact pads. Due to the LMA−AgNW biphasic structure of interconnection, the LMA is hermetically sealed by a homogeneous interface, realizing complete leak-free characteristics. Furthermore, integration reliability is successfully achieved by local strain control of the stretchable substrate with a selective glass fiber reinforcement (GFR). A strain localization derived by GFR makes almost 50,000% of strain difference within the board, and the amount of deformation applied to the constituent elements can be engineered. We finally demonstrated that the proposed integrated platform can be utilized as a universal s-PCB capable of integrating rigid/conventional electronic components and soft material-based functional elements with negligible signal distortion under various mechanical deformations.

KEYWORDS: stretchable electronics, printed circuit board, liquid metal, silver nanowire, modulus gradient
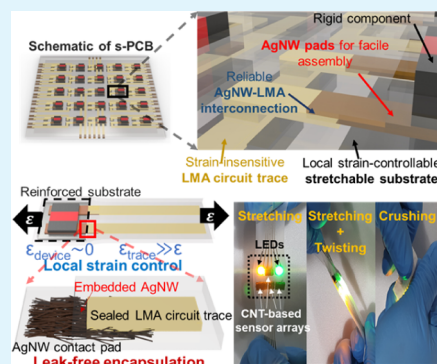
■ INTRODUCTION

Stretchable electronics has received significant attention as a promising alternative to conventional rigid electronics, particularly for the next-generation human-friendly electronic applications. As the interest and demand increase, a variety of stretchable electronic devices have been developed by implementing various unconventional electronic materials to stretchable polymers.[1−4] For the realization of stretchable electronics, it is necessary to raise to the system level beyond the single-device technologies. An electronic system in which all components such as substrates, circuits, IC chips, and passive/active elements are stretchable is considered the most ideal form of stretchable electronics. However, due to the limitations of the current technology, a reliable and all-stretchable electronic system is practically impossible to implement. A realistic form of the state-of-the-art stretchable electronic system is the integration of the conventional technology-based highly reliable functional components with a stretchable platform composed of a stretchable substrate and interconnections, namely, a stretchable integrated system. In the last decade, these multi-functional stretchable integrated systems have been actively introduced and widely utilized as health monitoring systems, prosthetics, smart clothes, and soft robotics.[5−7]

The paramount issue for these stretchable electronic systems with rigid components integrated with a stretchable platform is the mechanical and electrical reliabilities. Several approaches have been reported to improve the reliability of the system with prospects for development of the stretchable electronic platform composed of (i) stretchable interconnections and (ii) a stretchable substrate. One of the representative methods to produce stretchable interconnections is implementing structural designs to stiff polymeric films such a serpentine or kirigami structures to tolerate the applied strain.[8,9] The interconnections utilizing these structures showed a reliable electrical performance under mechanical deformation due to the structural stretchability of the stiff substrates and the electrical reliability of the metallic material deposited on them. However, this stretchable interconnection is based on the rigid material and has potential for interfacial failure between neighboring heterogeneous materials. In the electronic devices using this approach, poor long-term reliability of the metal thin film deposited on the stiff polymer such as polyimide (PI) and the delamination problem of the PI from the elastomeric substrate have frequently been addressed.[10] It is attributed to
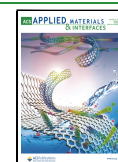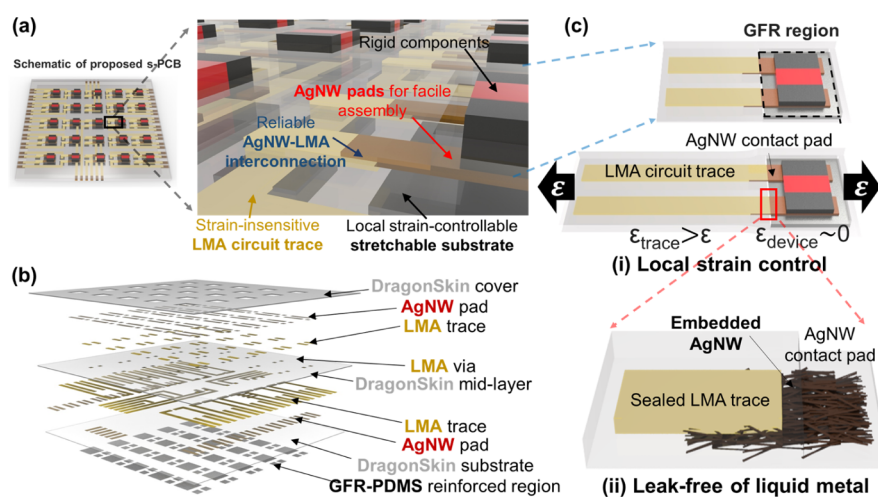
Figure 1. Structure of the s-PCB. (a) Schematic structure of the s-PCB that is composed of AgNW contact pads, LMA circuit traces, and the stretchable substrate with glass fiber-reinforced regions. (b) Multi-layer view of the s-PCB with properly positioned elements, leading to a synergistic effect of micro-/nanofunctional materials and polymer composites. (c) Unit structure of the s-PCB including two strategies for reliability enhancement: (i) local strain control and (ii) leak-free encapsulation of the LMA.

the mismatch of mechanical properties between adjacent materials, that is, soft−rigid interfaces. Utilization of liquid metals (LMs) is another promising method to make stretchable interconnections due to their intrinsic characteristics of electrical reliability and high conductivity.[11−14] For instance, Jeong, et al. reported an LM-based stretchable integrated system for wireless human motion monitoring.[12] However, the conventional LM-based stretchable electronics herein has a crucial problem, that is, the leakage of the liquid, leading to a gradual degradation of the device performance and eventually an electrical failure. The leakage commonly happens at the junctions between adjacent materials having different mechanical properties, that is, heterogeneous interfaces between a soft polymeric substrate and a stiff electrode, due to a deficient bonding strength to sustain stresses derived by external deformations.

In the aspect of stretchable substrates, a typical method for improving the reliability is the formation of stiff islands at selective areas.[15,16] When the substrate is composed of multi-materials with different moduli in certain regions, the strains applied to the stiffer islands become suppressed. The electrical components integrated with the stiff regions undergo minimal strain, leading to enhanced stability for device mounting. Several research studies reported this strain-island approach for a system-level integration including rigid resistors, capacitors, ICs, and PI−metal-based interconnections.[17−20] However, with this approach, the structural stability of the substrate itself can be weakened due to the local stress concentration at the interfacial area under stretching conditions.[21] It means that a trade-off between the device mounting stability and the intra-structural reliability of the substrate should be considered. In order to maximize the device integration stability, the difference in the mechanical properties between stiffened and pristine materials of the substrate should be significant. On the other hand, as the difference in the stiffness becomes larger, the potential of the interfacial failure increases like the situation of soft−rigid interfaces, resulting in poor intra-structural reliability. These reliability issues of the stretchable electronic platform originate from a heterogeneity of interfaces inherent in the overall stretchable device and limit the utilization of stretchable electronics in practical applications.

Here, to resolve the above-explained reliability issues of the stretchable systems, we suggest a reliable and stretchable electronic platform in the form of the printed circuit board (PCB) based on Ag nanowire (AgNW)−LM amalgam (LMA) interconnections and a modulus-gradient stretchable substrate. In order to achieve improved reliability of the stretchable integrated system, we minimized all possible heterogeneity at the interfaces. First, in order to secure both intra-structural stability and device mounting stability, a glass fiber reinforcement (GFR)-based modulus-gradient structure was employed in the stretchable substrate. Second, we realized a leak-free characteristic of the LM using AgNW-embedded elastomer composite structures as the interconnects between the LMA traces and the AgNW contact pads, resulting in the LM being hermetically sealed by a homogeneous matrix. Finally, we successfully fabricated a stretchable PCB (s-PCB) and demonstrated that both conventional rigid electronic components and soft material-based functional elements can be reliably integrated with the s-PCB with minimal signal distortion under mechanical deformations.

■ RESULTS AND DISCUSSION

An overall schematic structure of the s-PCB that consists of the LM-based circuit traces, AgNW contact pads, and elastomeric stretchable substrates with GFR regions is illustrated in Figure 1a. Dragon Skin (DS), one of the soft elastomeric polymers, was utilized as the substrate to provide high stretchability to s-PCB. DS showed a relatively low level of hysteresis ($\sim$6%) and good linearity ($R^2 \sim 0.99$) under 100% strain, even though more significant viscoelastic behavior could be observed under a larger level of strains due to the nature of the material, as plotted in Figure S1 (Supporting Information). As the circuit traces of the s-PCB, LMA, which is a metal particle-internalized Ga-based LM, was used for stable and stretchable electrodes. The contact pads for robust and easy integration of other functional electronic components were constructed by AgNW networks, which lead to a highly conductive metallic film. AgNW contact pads and LMA circuit traces are partially overlapped to make an electrical connection between them. As shown in the multi-layer view of Figure 1b, all the elements of the s-PCB are positioned and aligned at designated areas to
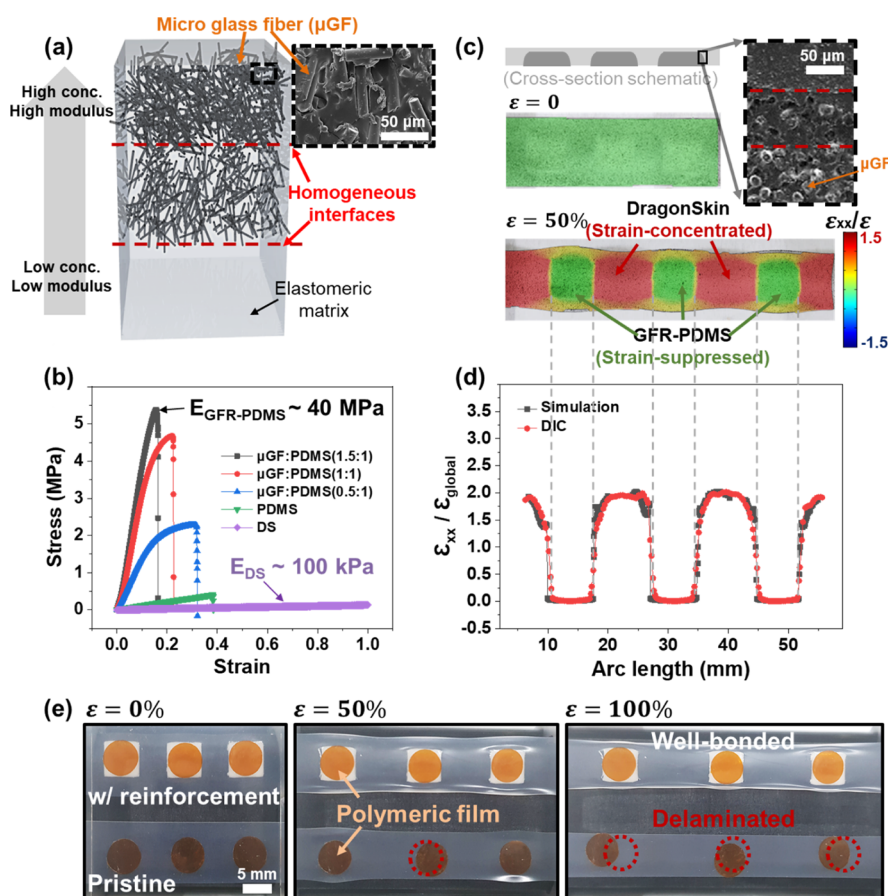
Figure 2. Characterization of the modulus-gradient stretchable substrate. (a) Schematic illustration showing the concept of the GFRP having homogeneous interfaces between the matrices with different elastic moduli. (b) Stress−strain curves of various polymeric composites with varied ratios of the added μGFs. (c) Graphical results of DIC analysis of the stretchable substrates with and without reinforcement. (d) Quantitative analysis of the DIC of the modulus-gradient substrate, showing the distribution of the strain without sharp changes at the interfaces. (e) Mounting stability of the modulus-gradient substrate, showing that the polymeric film attached to the reinforced region still adheres to the substrate, even when 100% strain was applied.

obtain a synergistic effect of the micro-/nanofunctional materials and polymeric composites. A cross-section schematic of the simplified unit structure with properly organized elements of the s-PCB is illustrated in Figure S2. The via structures in the mid-layer provide a high device integration density to the s-PCB like a conventional PCB. The synergy of these individual elements realizes the electrical/mechanical reliability of s-PCB that enables one to reliably integrate various electronic components with a universal stretchable platform.

In Figure 1c, two strategies for securing the reliability of s-PCB are explained as (i) the modulus-gradient substrate for local strain control and (ii) the AgNW−LMA biphasic interconnection for realizing no leakage of LM. Selective areas of the stretchable substrate were mechanically reinforced by a method of GFR to locally control the strain and stress within the s-PCB. It leads to an improved stability by repressing the strains applied to relatively vulnerable elements of s-PCB such as AgNW contact pads and via structures. For the reliable mounting of electronic components, integration slots of the s-PCB are also reinforced because minimal deformations should be applied to the integrated components. Although the larger strain is correspondingly applied at the circuit traces that are positioned in the substrate without GFR, a strain insensitivity of the LMA can maintain a high

conductivity required for the circuit traces. Furthermore, due to an embedded structure of AgNW percolation networks in DS at the interconnection between LMA traces and AgNW pads, the LMA can be hermetically sealed by the homogeneous DS matrix of the substrate and the leakage problem of the LM can be prevented.

A concept of the glass fiber-reinforced polymer (GFRP) that was utilized for the modulus-gradient stretchable substrate of the s-PCB is described in Figure 2a. Among several methods for modification of mechanical properties of the elastomeric polymer,[22−24] the method of GFRP is the one of the most facile approaches. This strategy has another important advantage of forming a reliable interface between matrices having distinct mechanical properties. Generally, an interface of two different materials (i.e., heterogeneous interface) is structurally unstable since a mismatch of mechanical properties causes dramatic changes of stresses under deformation.[21] A harsh deformation would result in a structural failure or delamination due to adhesion-based low bonding strength between the heterogeneous materials. On the other hand, the interface formed by the method of GFRP is homogeneous and the bonding strength is much larger than that of heterogeneous interfaces, resulting in lowering a possibility of the interfacial failure.

In Figure 2b, stress–strain curves of the GFRP composites with varied fractions of the added micro-glass fiber (μGF) into polydimethylsiloxane (PDMS) are plotted. The weight percent of μGF versus PDMS was changed, while other process conditions for the preparation of the glass fiber-reinforced PDMS (GFR−PDMS) composite were fixed (details are provided in the Experimental Section). As shown in the stress–strain plot, the mechanical properties of the composite are tuned by the addition of μGFs in terms of elastic modulus and stretchability. When the μGFs are mixed to PDMS with a weight ratio of μGF/PDMS = 1.5:1, the elastic modulus at 10% strain of the composite is 38.5 MPa. When compared with the pristine DS, which is softer than PDMS, the difference of the elastic modulus reaches about 400 times. Although the stretchability of the GFR−PDMS composite with a mixing ratio of 1.5:1 decreased with a failure strain of 16%, the local strain applied to the reinforced composite is substantially lower than the global strain within the entire modulus-gradient structure.

In order to estimate the strain distribution within the modulus-gradient stretchable substrate, a finite element method-based numerical simulation was conducted as presented in Figure S3. The material properties of the GFR−PDMS domain for the simulation were obtained from the fitting results of the uniaxial tensile test. Among the several hyperelastic solid models, the Mooney−Rivlin model with five parameters was the most closely fitted as shown in Figure S4, and we extracted material parameters from the results. The result of the simulation indicates that the strain profiles of the reinforced and pristine areas are obviously different with strain minimization and concentration, respectively. As the difference of the elastic moduli between the reinforced and pristine areas increased, the strain localization effect became more significant.

It should be proved that the deformation tendency predicted by the numerical simulation is realized in real fabricated samples. A simplified modulus-gradient structure was fabricated by patterning the GFR−PDMS composite with a square shape and covering this with a pristine DS thin film as explained in Figure S5. The GFR−PDMS was formed by several steps of thermal curing for the gradient concentration of the μGF including partial solidification, reflowing, and full curing as depicted in Figure S6. The microscopy images of the fabricated substrate showed not only a dome-like shape of the GFR−PDMS domain but also a μGF density gradient along lateral and vertical directions, realizing the gradient modulus within the substrate as shown in Figure S7. For acquiring actual values of local strains applied to the modulus-gradient stretchable substrate, digital image correlation (DIC) analysis was used as shown in Figure 2c,d. As expected, the strain distribution was apparently modified by partially introducing the reinforced composite matrices and the tendency of deformation was similar to the results of the simulation. In the reinforced area, a local strain of only 0.2% was measured, while a global strain of 50% was applied to the whole structure. At the same time, the strain-concentrated region (i.e., non-reinforced region with pristine DS only) experienced almost doubled values of local strain with respect to the global strain. Remarkably, the disparity of the local strains observed by both simulation and DIC was ~50,000% within the substrate, that is, the actual values of minimum and maximum strains are 0.211 and 102.7% in the simulation and similarly 0.201 and 100.5% in the DIC, respectively. Furthermore, the interfaces

between two different matrices with and without μGFs showed a gradual transition, not a sharp change, of the local strain. Comparison in terms of structural failure and the strain profile of the μGF-incorporated stretchable substrates with different GFR−PDMS structures is depicted in Figure S8. In the case without the gradient structure of GFR−PDMS, the reinforced domain was delaminated at 260%, which was much lower level than the material failure strain, and the sharp profiles at the interfaces were shown. However, the modulus-gradient substrate showed a structural fracture at 490% strain and smoothly changed strain profiles. This gradient strain profile enhanced structural stability by preventing an easy interfacial failure that originated from a dramatic change of mechanical properties. Note that the smooth profile of strains can be realized by a facile one-step screen printing process, while conventional rigid island approaches for strain localization require multiple steps of fabrication processes.[25−27] Considering these results, it is confirmed that the strain profile of the stretchable substrate having a partially introduced GFRP composite is locally controllable and the amount of the restrained and concentrated strains is dependent on the fraction of the incorporated μGFs.

When a complex deformation such as an omnidirectional strain is applied to the modulus-gradient substrate, similar aspects are observed as shown in Figure S9. The substrate with 2-D arrayed patterns of the reinforced composite was stretched omnidirectionally and analyzed using DIC and a numerical simulation. According to the results of DIC analysis, the local principal strains at the reinforced and pristine regions of the sample were ~0.003 and 2.8 times of the global omnidirectional strain, respectively. This strain-suppressed tendency was well matched to the results of the numerical simulation that was conducted by 3-D modeling having hyperelastic material properties of the tested sample. It implies that the modulus-gradient structure is able to retain its characteristics of local strain control under complicated stretching conditions.

The locally suppressed strain of the stretchable substrate leads to an integration reliability. In Figure 2e, identical polymeric films were attached on two different stretchable substrates, one with modulus-gradient structures (upper) and another without them (lower). The polymeric film mounted on the pristine stretchable substrate started to delaminate from the substrate under a global strain of 50%. However, the polymeric film attached to the reinforced area of the modulus-gradient substrate was well bonded even at a global strain of 100% since the actually applied local strain is only about 0.4%. Due to the locally reinforced substrate having an intermediate value of Young's modulus (~40 MPa), the polymeric film mounted on this region was not detached, even though the mechanical mismatch between the film and mother substrate is huge with Young's moduli of 2.5 GPa and 100 kPa, respectively (Supporting Information Video 1).

LM, which is one of the representative materials for stretchable electrical interconnections, was implemented as a highly conductive and stretchable circuit trace of the s-PCB. However, general Ga-based LM retains several obstacles for practical uses in stretchable electronics. First, poor wettability of the LM, especially to the elastomeric polymer substrate, inhibits a facile utilization as conductive elements of electronic devices and impedes the degree of freedom of the fabrication process. The wetting property of the LM originates from its high surface tension so that plasma treatment[28] or additional layers for promoting adhesion have been required to reliably

utilize the LM for stretchable platforms.[29−31] As an alternative simple approach to improve the wettability and processability of LM, we internalized metallic particles into the LM, resulting in a solid−liquid transitional material, so-called LMA.[32] Tang et al. reported the research about the transitional-state metallic mixture of Ga-based LM with Cu particles. Ga becomes electrochemically reactive in an acidic or alkaline medium, forming $Ga(OH)_3$ or Ga_2O_3, respectively, owing to its low reduction potential. Thus, the Ga-based LM spontaneously interacts with the metal ions such as Fe^{3+}, Ni^{2+}, and Cu^{2+} in solution. Here, Cu particles were impregnated to Galinstan and the $CuGa_2$ intermetallic compound was formed at the Ga−Cu interfaces by a redox reaction.[33,34] Due to their semi-solid state, a bridging phenomenon of LM through the internalized particles is revealed. It leads to the suppression of the nature of LM to be gathered and to the enlargement of the surface area to be contacted to the target substrate. It means that the adhesion characteristics of the LM, such as wettability, are improved as illustrated in Figure 3a. Moreover, the LMA is

Figure 3. Preparation of LMA. (a) Schematic illustration for the comparison of wettability between the LM and LMA. (b) Photographic images showing procedures for preparation of the LMA. (c) SEM images showing different microscopic morphologies of LMA, whose solidity increases with a portion of Cu particles.

well wetted to the AgNW film, which is essential to make sure a reliable electrical connection from the LMA circuit traces to the AgNW contact pads of the s-PCB.

Characterization of the LMA was conducted to verify the process compatibility in the fabrication of the s-PCB. A series of procedures, including a reduction of surface oxide layers surrounding Cu particles and Galinstan and the production of Cu−Ga chemical compounds, were proceeded as presented in Figure 3b. As a result of this process, LMA with a transitional state between the liquid and solid was produced. It was observed that higher solidity of the LMA was obtained by internalizing more Cu particles. Scanning electron microscopy (SEM) images in Figure 3c show the distinct microscopic morphology of the LMA with respect to the weight percentage of the added Cu particles. The inclusion of the Cu particles

enhanced the wetting property of the LM due to the effects of the enlarged contact area and a bridging phenomenon.[32] However, when the fraction of Cu was over a certain value, herein, 15 wt %, Cu-rich regions, wherein solid-like properties prevail, were widely observed, leading to restraining the wetting of the LMA. Consequently, the LMA having 10 wt % Cu particles was selected for the circuit traces of the s-PCB by considering the conductivity, strain insensitivity, reliability, and processability.

The second consideration for practical uses of LM in stretchable electronics is the leakage causing a gradual degradation of the device performance and an electrical failure. In Figure 4a, a schematic structure to inhibit the leakage of the LM is proposed. The strategy for realizing leak-free characteristics is to make the LMA circuit trace sealed by a homogeneous elastomeric matrix. Although the LMA was entirely encapsulated, an electrical extension to form the interconnection was fulfilled by AgNW percolation networks embedded in the elastomeric substrate. As an element of the s-PCB, the AgNW network connecting with LMA can be utilized as the contact pads for the integration of other devices and components.

The SEM images of the proposed AgNW−LMA interconnection structure are shown in Figure 4b. Note that the interconnection formed by overlapping AgNWs and LMA was entirely covered by the homogeneous matrix of DS as shown in the yellow-dashed part and an electrical pathway was extended through the AgNW with the form of the percolation networks as observed in the inset image of the blue-dotted box. The microinspection of the AgNW−LMA interconnection structure proved that the LMA circuit trace is hermetically sealed for the prevention of leakage, maintaining the electrical connection with the AgNW contact pad at the same time. For further investigation of the leak-free characteristic of the AgNW−LMA interconnection, it was compared to the case of using Cu tape instead of AgNW networks. Supporting Information Video 2 shows that the LMA interconnected with the Cu tape is leaked by intensively applied pressure through the heterogeneous interfaces between Cu tape and the DS substrate, while the LMA with the AgNW interconnection is not leaked at all under a similar amount of pressing force as shown in Figure S10.

The electrical reliability of the AgNW−LMA interconnection and the effect of the modulus-gradient structure were verified using a uniaxial stretching test as presented in Figure 4c,d. A schematic configuration for the test is depicted in Figure S11a (details of fabrication processes are explained in the Experiment Section). In the case without any modulus reinforcement of the substrate, that is, pristine DS substrate, the $\Delta R/R_0$ values of the interconnection dramatically increased by ∼40 times under a strain of 50%. Although the AgNW has strain-sensitive characteristics, the sensitivity can be tuned by controlling the local strain applied at the AgNW-patterned area. When a modulus-reinforced composite matrix was formed underneath the AgNW networks, the local strain applied to AgNW could be restrained and its resistance change could be minimized. The strain insensitivity of AgNW is dependent on the density of μGFs embedded in the reinforced composite. As the weight fraction of the μGF with respect to PDMS increased from 0.5 to 1.5, $\Delta R/R_0$ of the AgNW pad was dramatically reduced from 12.7 to 0.27. For actual uses of the AgNW−LMA interconnection as the elements of the s-PCB, the absolute resistance value should also be considered. In
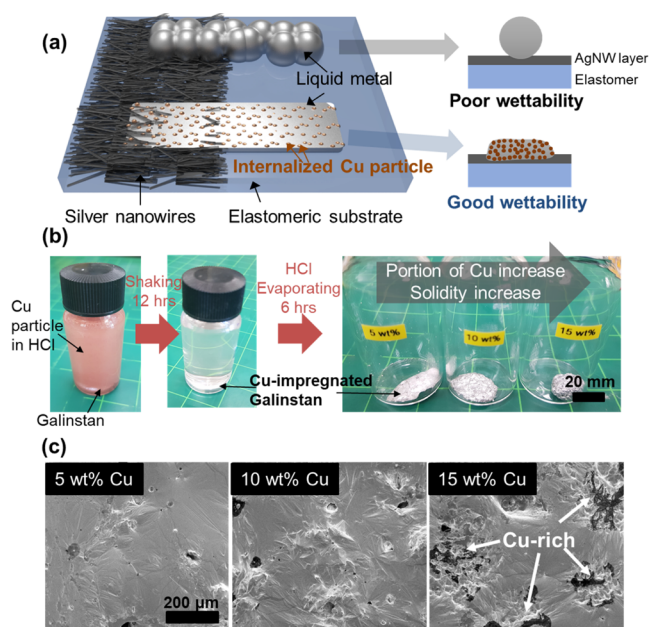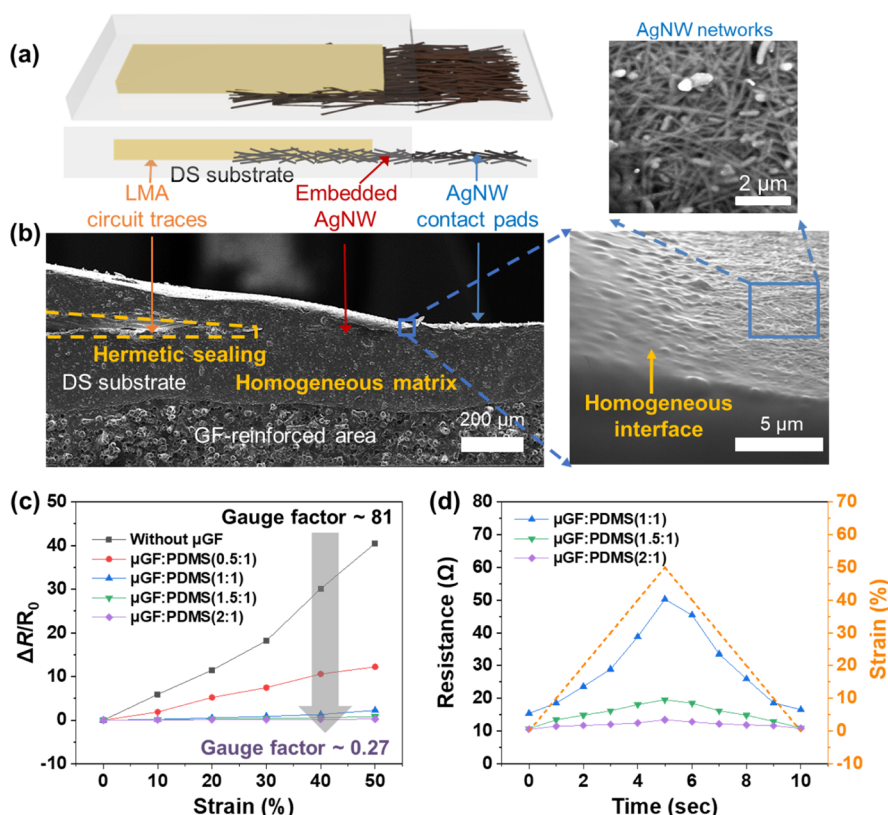
Figure 4. Characterization of the AgNW−LMA interconnect. (a) Schematic illustration of a structure for a leak-free characteristic of LMA derived from a homogeneous sealing of the LMA using the embedded structure of AgNW networks. (b) SEM images of the proposed AgNW−LMA interconnect structure, proving that the LMA is hermetically encapsulated and makes a contact with the AgNW networks due to their embedded structure. Strain-induced changes of the (c) normalized and (d) absolute resistances of the AgNW networks with respect to the fraction of the μGFs included in the mechanically reinforced substrate.
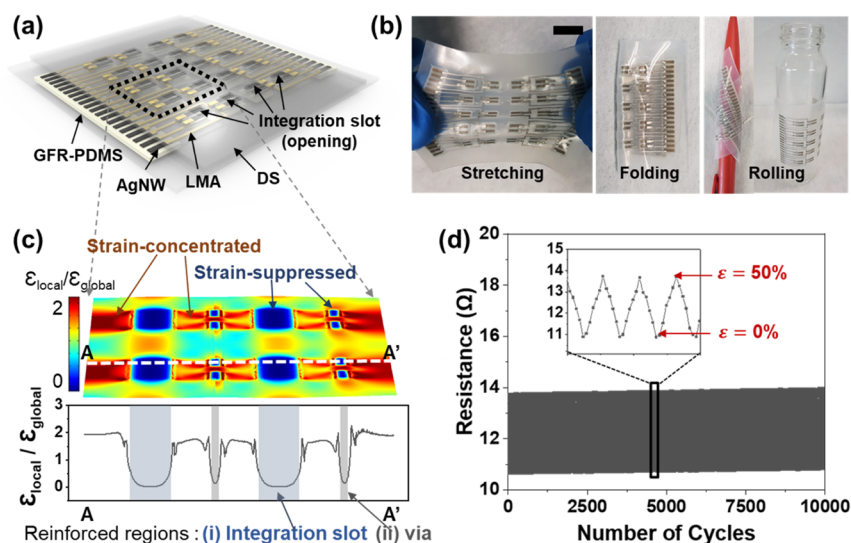

Figure 5. Fabrication and characterization of s-PCB. (a) Schematic illustration of the s-PCB prototype. (b) Photographic images of the fabricated s-PCB under various deformations (scale bar: 10 mm). (c) Results of a numerical simulation with a 3-D model of the s-PCB. A clear distinction between the strain-concentrated and suppressed areas due to the selective GFR within the substrate is observed. (d) Long-term reliability test of the unit structure of the s-PCB. The s-PCB was stretched with a strain rate of 0.1 s^{-1} during the repeated cyclic tests.

Figure 4d, the absolute resistance of the interconnection was measured as a 10 Ω level and its increment under 50% strain was only a few ohms when the GFR−PDMS composites existed as the support. It means that the AgNW−LMA bimaterial structure is suitable and reliable as the electrical

elements of the s-PCB from circuit traces to contact pads when conjugating with the modulus-gradient stretchable substrate.

In Figure 5a, a schematic structure of the s-PCB prototype, which is the fabricated by processes explained in Figure S12, is illustrated (details of the fabrication process are explained in
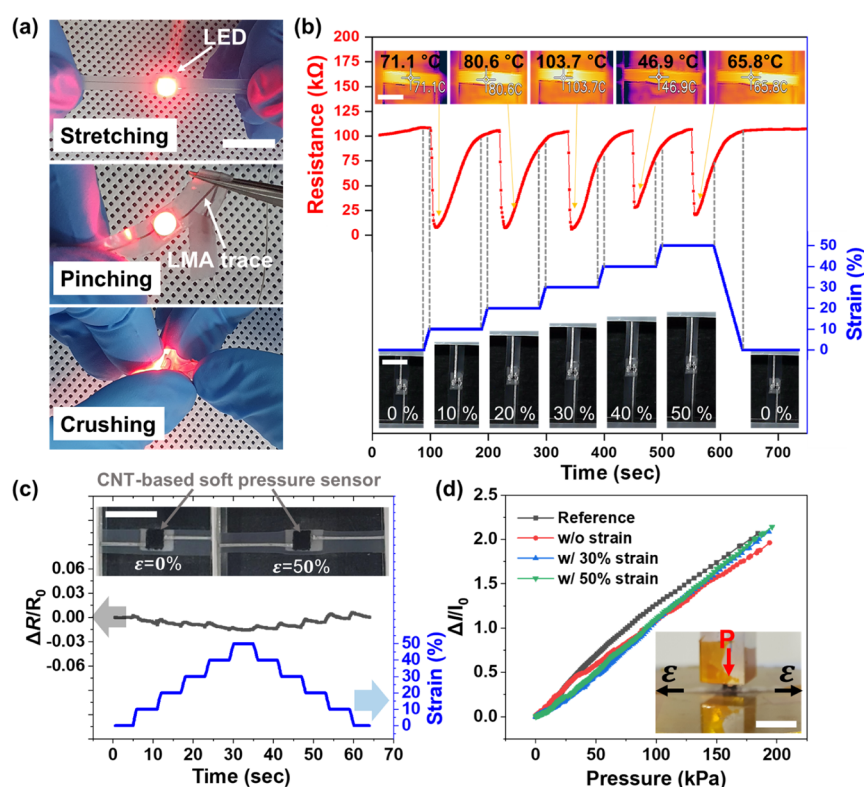
Figure 6. Integration performance of s-PCB. (a) Photographic images showing that the light intensity of the integrated LED is maintained under various harsh deformations. (b) Responses of the integrated chip thermistor, which are only dependent on the heat regardless of dynamic strain profiles. (c) Normalized resistance of the integrated CNT-based soft pressure sensor under varying strain conditions. (d) Pressure-sensitive and strain-insensitive responses of the integrated soft sensors under stretched states of the s-PCB. All the scale bars in the photographic images are 10 mm.

the Experimental Section). The overall fabrication processes could be divided by the formations of the bottom, top, and intermediate layers of the s-PCB as described in the schematic of Figure 1b. Electrically vulnerable parts such as the via structures and the AgNW–LMA interconnections were arranged onto the GFR–PDMS patterns, while the robust and deformation-insensitive LMA circuit traces were formed in the locations irrespective of the reinforcement of the substrate. The photographic images of the fabricated s-PCB under different deformation conditions are presented in Figure 5b. The s-PCB was reliably deformed under stretching, bending, folding, and rolling without any structural failure or delamination of heterogeneous interfaces. Notably, no leakage of the LMA was observed, even though harsh deformation occurred at the s-PCB.

Before practical uses of the s-PCB prototype, further numerical simulation was conducted with conditions depicted in Figure S13 to check a strain distribution on the s-PCB with the multi-layer configurations. It was assumed that the mechanical properties of the AgNW embedded-elastomer (i.e., contact pads) were the same as those of the substrate and the LMA was replaced with air considering incompressible characteristics of the liquid. As graphical and quantitative results in Figure 5c, the strain distribution within the s-PCB can be tuned by the selective reinforcement of the substrate. When checking the strain profile along the white-dotted line (A–A′) in the schematic, the integration slots and the via holes positioned upon the GFR–PDMS underwent relatively small amounts of strains with minimum values of 0.2% under a global strain of 10%, while larger strains were observed at the

substrate without mechanical reinforcement. Although electrical elements of the s-PCB (i.e., LMA and AgNW) have different sensitivities under deformations, it is proved by the simulation that the local strain-controllable substrate and a systematic organization of the elements can attribute to an improvement of the reliability of the integrated stretchable platform.

In Figure 5d, the long-term reliability of the structure of the s-PCB is investigated. The configuration of the tested structure is shown in Figure S11b. The Ag epoxy that was used for a conductive adhesive to integrate other devices was applied to the AgNW contact pads. We could also check the stability of the "device-to-contact pad" interconnections, considering that the applied Ag epoxy is a fragile low-resistance material. The initial resistance of the tested structure showed ~10 Ω, confirming an electrical connection between the top and bottom circuit traces through the via holes. During 10,000 times loading and unloading cycles with a strain of 50%, the amplitude of responses maintained with only a 1.6% drift of the base resistance. The strain-induced change of the resistance was ~2.5 Ω, which was an acceptable value when considering the initial resistance and sensitivity of the devices to be integrated.

Integration performances of the s-PCB as a stretchable electronic platform were investigated. First, rigid commercial devices such as a surface mountable light-emitting diode (LED) and a chip thermistor were mounted onto the s-PCB and their performances were evaluated after integration. The integrated LEDs were stably brightened maintaining an intensity of the light, even though harsh deformations were
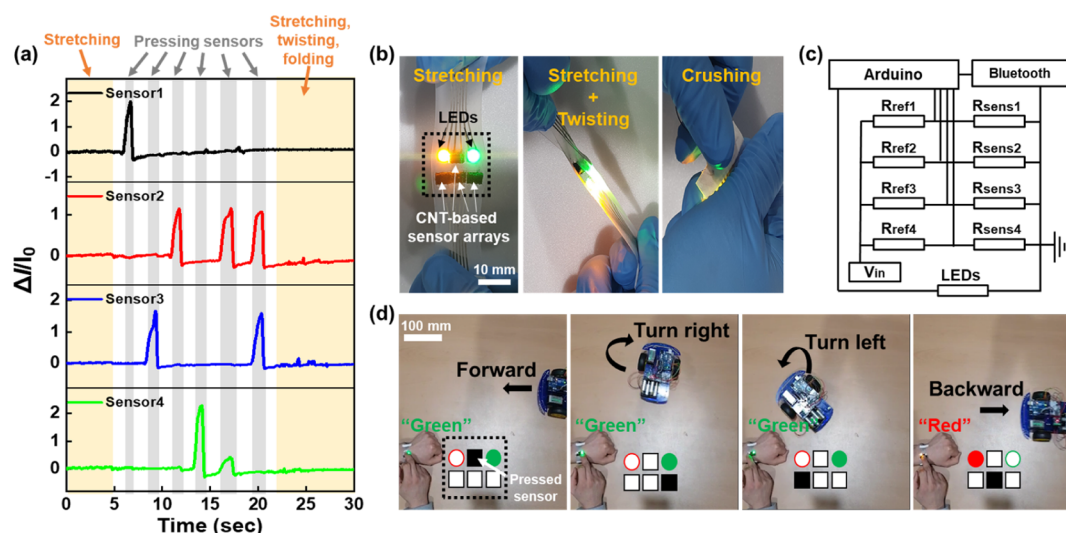
Figure 7. Multi-functionality implemented with the s-PCB. (a) Responses of four CNT-based soft pressure sensors integrated with the s-PCB under the sequential mechanical stimulus. (b) Soft and rigid multi-devices showing high integration reliability without any mechanical/electrical failure under harsh deformations occurring in the integrated stretchable platform. (c) Circuit diagram for operating an RC model car using an integrated system realized by multi-components mounted on the s-PCB. (d) Demonstration of the RC car control using a multiple pressure sensor array on the s-PCB.

applied to the s-PCB like stretching, pinching, and crushing as shown in Figure 6a. No leakage of the LMA was observed while handling and applying external forces. In Figure 6b, a chip thermistor was mounted on the s-PCB and multiple stimuli (i.e., strains and heats) were applied at the same time. While the s-PCB was stretched with arbitrary strain profiles, the integrated negative temperature efficient (NTC) thermistor retained its thermal-responsive characteristics, showing a resistance drop only by the heating regardless of the deformation of the s-PCB. This result proves that the integrated devices provide their designated functions stably without signal disturbances under stretching of the integrated platform.

The performance of the s-PCB in the case of integrating soft material-based functional devices was also examined. The used device was a carbon nanotube (CNT)-based soft pressure sensor with microporous structures, which was reported previously.[35] The pressure sensor consists of a microporous elastomeric template and CNTs coated on its surfaces and internally located pores. As the pores are closed by pressure, the CNTs make more electrical paths and the electrical resistances become decreased. Due to the porous structures, the sensor showed improved sensitivity, hysteresis, and long-term stability compared to the CNT-coated bulk elastomer without any pores. The base resistance of the soft pressure sensor was well perseveres at the initial value after integration with the s-PCB. In the stretching situation of the s-PCB, a normalized resistance was slightly changed with a maximum value of 1.5% under varied strains ranging from 0 to 50% despite the fact that the integrated sensor was made from ultra-soft materials and structures, as shown in Figure 6c. It was attributed to the strain suppression of the integration region, resulting in a negligible strain applied to the soft pressure sensor. Furthermore, pressure-sensitive and strain-insensitive responses of the integrated sensor are investigated in Figure 6d. The soft pressure sensor mounted on the integration slot of the s-PCB was pressed by an insulator tip installed on a universal tensile/compressive testing instrument. The integrated platform had different statuses with strains of 0, 30, and

50% when the pressing procedure was conducted. All the pressure-sensitive responses of the sensor showed a similar tendency regardless of the amount of the strains applied to the s-PCB. It is remarkable that not only the conventional rigid components but also the soft material-based functional devices are reliably integrated without a signal distortion that can be derived by the unwanted mechanical stimuli owing to the reliable structure of the electrical elements (i.e., AgNW-LMA interconnect) and strain-localization characteristics of the substrate of the s-PCB.

It is necessary to realize the multi-functionalities of the integrated system beyond the reliable operation of a single component. In Figure 7, multi-functionalities based on multi-devices integrated with the s-PCB were realized. Four CNT-based soft pressure sensors and two commercial LEDs were mounted on the s-PCB and operated their functions. The integrated sensors provided pressure-sensitive characteristics, even though various deformations such as stretching, twisting, crushing, and folding were applied to the entire stretchable system as shown in Figure 7a (Supporting Information Video 3). At the early stage of the experiment around 0 to 5 s, all the sensors did not respond while the integrated platform was stretched by a strain of ~70%. After that, sequential inputs of pressure were applied to the sensors, and their responses were clearly confirmed without signal interference between adjacent components. Then, various deformations were applied to the platform, and the sensors showed negligible changes in signals. In Figure 7b, photographic images showed multi-devices integrated with the s-PCB under different deformations. Two LEDs were reliably brightened, and four pressure sensors were stably mounted without delamination or detachment despite harsh deformations occurring at the integrated platforms.

As a wearable application of the integrated s-PCB, we demonstrated a wearable user interface device that could remote-control a model car using the Arduino and Bluetooth module with a circuit diagram shown in Figure 7c. We designated that each CNT-based pressure sensor made four different driving modes of the model car and LEDs turned on during movement of the car as shown in Figure 7d (Supporting

Information Video 4). Mimicking the keyboard's arrow keys, pressing the sensor positioned at the upper central region of the integration area (i.e., dotted-box area) made the model car move forward and the green LED turn on. In the same notion, when the sensors formed on the right and left positions were pressed, the model car turned right and left, respectively. In the case of pressing the lower-center sensor, the car moved backward and the red LED turned on simultaneously.

CONCLUSIONS

In summary, we developed a reliable and stretchable printed circuit board composed of AgNW contact pads, LMA circuit traces, and a selectively reinforced DS stretchable substrate. Reliability, which is of paramount importance in stretchable electronics, could be achieved by the control of local strains applied to the substrate and the prevention of the leakage of the LM. The elastic modulus of the substrate was partially modified by the method of GFR, leading to a suppression of the strains applied at vulnerable internal structures and integration slots of the s-PCB. For the leak-free characteristics, the LMA for the circuit traces was hermetically encapsulated by the DS matrix with homogeneous interfaces, forming seamless interconnections with the embedded AgNW structure for an electrical connection to the AgNW contact pads. The systematic arrangement of these elements of the s-PCB enables both the intra-structural stability and the mounting stability of the integrated devices. The s-PCB successfully integrated not only rigid but also soft electronic devices without signal distortions under various external stimuli. Finally, it was demonstrated that the wearable electronic system implemented by the multiple component-integrated s-PCB could be utilized for the control of a remote-controllable (RC) model car. We believe that the s-PCB can be a breakthrough for the transition from rigid to stretchable electronics by serving as a universal electronic board for easy and reliable integration of various electronic devices.

EXPERIMENTAL SECTION

Preparation and Characterization of the GFRP Composite. In order to prepare the glass GFRP composite, μGFs and PDMS were blended using a planetary mixer (ARE-310, Thinky Inc., USA). The GFs (MF300, Fiber Man Co., Korea) having average values of 300 μm of length and 13.5 μm of diameter were incorporated in the liquid-state uncured PDMS (Sylgard 184, Dow Corning Co., USA) including a curing agent with a ratio of 1:5. The mixed ratio of the μGF was varied by the values of 0.5, 1, 1.5, and 2 with respect to the weight of the PDMS precursor. The prepared elastomeric composite was molded in a standard shape for the rubber tensile test (ASTM D412) at 100 °C for 20 min to investigate its mechanical properties. The characterization was conducted using a tensile tester (AGS-X Series, Shimadzu Co., Japan). The acquired stress–strain curves were fitted to suitable hyperelastic models using Abaqus to analyze and extract parameters for the numerical simulation.

Fabrication of the Modulus-Gradient Stretchable Substrate. GFR–PDMS was patterned by screen printing on a Si wafer that was hydrophobic-treated for easy detachment of the elastomer. A shadow mask for the patterning was prepared by a programmed cutting of a polymeric sheet having a height of 300 μm using a plotter (Cameo 4, Silhouette America Inc., USA). The spatial resolution of GFR–PDMS is determined by a specification of the machine, about 200 μm here. After forming 300 μm thick GFR–PDMS patterns, the uncured liquid DS (Dragon Skin 10, Smooth On Inc., USA) was deposited by spin-coating at 800 rpm for 30 s. GFR–PDMS included a small portion of DS (a weight ratio of 1:25 to

PDMS) to enhance the bonding between GFR–PDMS and the DS substrate.

Digital Image Correlation for Strain Mapping. For DIC analysis, the specimen was patterned with a spray paint (Rust Oleum, USA). Then, we obtained optical microscopy images of the specimen before and after deformation using a digital camera (EOS 800D, Canon, Japan) that was firmly mounted on tripods. The taken digital images were processed using commercial DIC software (Aramis Professional, Gom GmbH). For the image processing, a subset size of 160 pixels and a subset distance of 80 pixels were used to achieve a high accuracy. The accuracy of the DIC was calculated as 0.05% (2 × displacement error/subset distance = 2 × 0.02 pixels/80 pixels).[36,37]

Preparation of LMA. Galinstan and Cu particles were used to make the LMA utilized as the stretchable circuit traces. Cu particles having an average diameter of 1 μm were put in a vial containing Galinstan with different weight fractions of 1, 5, 10, and 15% versus Galinstan. In order to break the interfacial barriers that originate from the surface oxide layers and to merge the Cu particles and Galinstan, hydrochloric acid (HCl) as a reducing agent was poured into the container. The container is shaken for 12 h for internalization of the Cu particles into the Galinstan. After the complete internalization, evaluated by the color change from opaque to transparent, the HCl solvent was removed and evaporated at 60 °C for 6 h in a vacuum chamber.

Reliability Test of the s-PCB. In order to evaluate the reliability of the elements of the s-PCB, the samples with different structure configurations illustrated in Figure S11 were loaded on a programmable linear actuating stage and fixed by foam tapes. The samples were stretched and released by the actuated stage. At the same time, the electrical resistance of the sample was measured using a source meter (2400, Keithley Instruments, USA) and the data were obtained by Labview Software (National Instruments, USA).

Fabrication of the s-PCB Prototype. The whole fabrication process is illustrated in Figure S12. The Si wafer was hydrophobic-treated by the perfluoropolyether solution process for easy detachment after the whole processes were done. First, the modulus-gradient substrate was prepared by the same process explained above except for a thickness and a GF fraction. For the prototype of the s-PCB, the reinforced part consisted of μGF/PDMS = 2:1 (w/w) and had a thickness of 500 μm. After partial curing of the spin-coated DS at room temperature for 1 h, a 1 wt % AgNW solution with the isopropyl alcohol solvent (Flexiowire 2020c, Flexio Co., Korea) was spray-coated on the prepared substrate with a polyethylene terephthalate mask for the formation of the contact pads. The critical dimensions of the AgNW patterns can be determined by an electrical bridging between adjacent patterns during the spraying process. The hydrophobic-treated mask was put on the precured DS substrate to make a strong adhesion and to minimize the gap between them. After spray coating of the AgNWs, the mask was detached from the DS substrate that was fully cured. The resolution of the patterns and the spacings was ~200 μm. The deposited AgNWs were annealed at 100 °C for 30 min. Then, the LMA trace patterns were formed with the existence of partially overlapped regions with AgNWs. The polymeric shadow mask for patterning LMA was prepared by the plotter, and the LMA was deposited by brushing after aligning the mask on the AgNW-patterned DS substrate. Then, the deposited LMA was screen-printed using slide glass for the formation of the thin conductive traces. After that, the DS was deposited again to form an intermediate layer. The via holes and AgNW contact pads were not covered but exposed in this process through a masked spin-coating process. After the room-temperature curing of the DS, structuring of the top layer including LMA traces, AgNW top pads, and the DS cover layer was conducted by the same processes for the bottom layer. The cover DS layer had integration slots for exposing the top AgNW contact pads.

Characterization of the Integration Performance. The LEDs (LS-SF5050-UE3-C, Zhejiang Guyue Longshan Electronic Technology Development Co., China) and negative temperature coefficient (NTC) chip thermistors (TSM2A104J4102RZA, Thinking Electronics Industrial Co., China) were mounted on the integration slots of the s-PCB using Ag epoxy (MG Chemicals Ltd., 8331S, Canada) as

a conductive adhesive. The Ag epoxy was applied to each contact pad of both the devices and s-PCB and sintered after mounting using a convection oven at 60 °C for 20 min. The mounted LED was turned on using a DC power supply (E3640A, Agilent Technologies Inc., USA). The mounted thermistors were electromechanically characterized by the same method as the section for the structural reliability test. Simultaneously, the thermistor mounted on the s-PCB was heated by a heat gun, and the corresponding temperature was measured using an infrared camera (FLIR ONE Pro, FLIR System Inc., Korea). The strain profile generated by the linear stage was programmed regardless of the heating pattern to check the decoupling characteristic of the s-PCB.

Operation of the RC Model Car. The motion of the RC model car was controlled by the wearable electronic system that was implemented by the s-PCB integrating functional devices. The same LEDs and CNT-based pressure sensors as used above were connected to AgNW contact pads of the s-PCB using an Ag epoxy. For the data acquisition and Bluetooth communication, two Arduino Uno boards were utilized: one on the RC car and another connected to four pressure sensors and two LEDs integrated with s-PCB. Each board was connected to a Bluetooth module (HC-05, Tenco Technology, USA). The module on the car was on the slave mode, and the other was on the master mode, which enabled a remote control. Voltage-divider circuits were utilized to measure the change in resistances of four pressure sensors. A situation of pressing each sensor sent the corresponding motion command to the RC car via Bluetooth communication. Moreover, in order to check the responses of the sensors and to verify the corresponding operation of the RC car, a red LED was turned on for the backward motion command and a green LED was on for other motions (forward, left turn, and right turn) of the RC car. When the Arduino Uno on the car received the command, it made two front wheels be driven by a motor system (L9110s, Shenzhen iSmart Electronic Co., China). The combination of directions of the two motors connected to each wheel allowed four distinct motions: driving forward, backward, turning left, and turning right. Arduino Uno on the car was powered with a 9 V battery, and the motor system was powered by four AA batteries.

■ ASSOCIATED CONTENT

ⓢ Supporting Information

The Supporting Information is available free of charge at https://pubs.acs.org/doi/10.1021/acsami.1c16177.

Hysteresis of DS 10 under different strains, cross section schematic of the simplified unit structure of the s-PCB with well-aligned elements, numerical simulation of the modulus-gradient substrate with different ratios of Young's moduli between reinforced (E1) and pristine areas (E0), fitting results of uniaxial tensile test data of the GFR−PDMS composite to several hyperelastic material models, fabrication processes of the modulus-gradient stretchable substrate, microscopic cross-sectional images of the fabricated modulus-gradient substrate, comparison between the μGF-incorporated stretchable substrate with and without the gradient structure of the GFR−PDMS domain, results of DIC and numerical simulation of the modulus-gradient substrate with 2-D array patterns, schematic configurations for the reliability test of the s-PCB, overall fabrication processes of the s-PCB, and numerical simulation conditions and hyperelastic material properties of the elements (PDF)

Mounting stability of the modulus-gradient substrate (MP4)

Leakage comparison between LMA−AgNW and LMA−Cu tape interconnections (MP4)

Multi-device operation (MP4)

Model car control via integrated s-PCB (MP4)

■ AUTHOR INFORMATION

Corresponding Authors

Hyuneui Lim − *Department of Nature-Inspired System and Application, Korea Institute of Machinery and Materials (KIMM), Daejeon 34103, Republic of Korea;* ⓘ orcid.org/0000-0003-2692-647X; Email: helim@kimm.re.kr

Inkyu Park − *Department of Mechanical Engineering, Korea Advanced Institute of Science and Technology (KAIST), Daejeon 34141, Republic of Korea;* ⓘ orcid.org/0000-0001-5761-7739; Email: inkyu@kaist.ac.kr

Authors

Min Seong Kim − *Department of Mechanical Engineering, Korea Advanced Institute of Science and Technology (KAIST), Daejeon 34141, Republic of Korea*

Seunghwan Kim − *Department of Mechanical Engineering, Korea Advanced Institute of Science and Technology (KAIST), Daejeon 34141, Republic of Korea*

Jungrak Choi − *Department of Mechanical Engineering, Korea Advanced Institute of Science and Technology (KAIST), Daejeon 34141, Republic of Korea*

Seonggi Kim − *Department of Nature-Inspired System and Application, Korea Institute of Machinery and Materials (KIMM), Daejeon 34103, Republic of Korea*

Chankyu Han − *Department of Mechanical Engineering, Korea Advanced Institute of Science and Technology (KAIST), Daejeon 34141, Republic of Korea*

Yung Lee − *Department of Materials Science and Engineering, Korea Advanced Institute of Science and Technology (KAIST), Daejeon 34141, Republic of Korea;* ⓘ orcid.org/0000-0003-3226-1937

Youngdo Jung − *Department of Nature-Inspired System and Application, Korea Institute of Machinery and Materials (KIMM), Daejeon 34103, Republic of Korea*

Jaeho Park − *Department of Mechanical Engineering, Korea Advanced Institute of Science and Technology (KAIST), Daejeon 34141, Republic of Korea;* ⓘ orcid.org/0000-0002-0213-8076

Sunjong Oh − *Department of Nature-Inspired System and Application, Korea Institute of Machinery and Materials (KIMM), Daejeon 34103, Republic of Korea*

Byeong-Soo Bae − *Department of Materials Science and Engineering, Korea Advanced Institute of Science and Technology (KAIST), Daejeon 34141, Republic of Korea;* ⓘ orcid.org/0000-0001-9424-1830

Complete contact information is available at:
https://pubs.acs.org/10.1021/acsami.1c16177

Author Contributions

The manuscript was written through contributions of all authors. All authors have given approval to the final version of the manuscript.

Notes
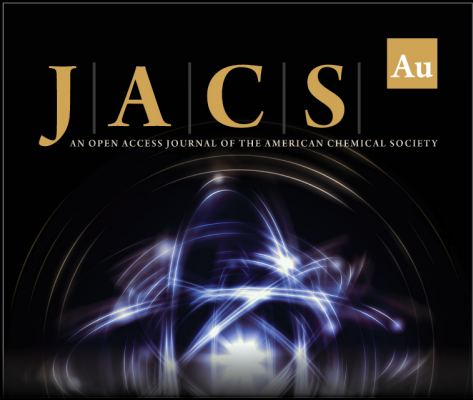
The authors declare no competing financial interest.

■ REFERENCES

(1) Amjadi, M.; Pichitpajongkit, A.; Lee, S.; Ryu, S.; Park, I. Highly Stretchable and Sensitive Strain Sensor Based on Silver Nanowire–Elastomer Nanocomposite. *ACS Nano* **2014**, *8*, 5154–5163.

(2) Lee, J.; Kim, S.; Lee, J.; Yang, D.; Park, B. C.; Ryu, S.; Park, I. A Stretchable Strain Sensor Based on a Metal Nanoparticle Thin Film for Human Motion Detection. *Nanoscale* **2014**, *6*, 11932–11939.

(3) Gu, J.; Kwon, D.; Ahn, J.; Park, I. Wearable Strain Sensors Using Light Transmittance Change of Carbon Nanotube-Embedded Elastomers with Microcracks. *ACS Appl. Mater. Interfaces* **2020**, *12*, 10908–10917.

(4) Kim, M. S.; Kim, K.; Kwon, D.; Kim, S.; Gu, J.; Oh, Y. S.; Park, I. Microdome-Induced Strain Localization for Biaxial Strain Decoupling toward Stretchable and Wearable Human Motion Detection. *Langmuir* **2020**, *36*, 8939–8946.

(5) Jang, K.-I.; Li, K.; Chung, H. U.; Xu, S.; Jung, H. N.; Yang, Y.; Kwak, J. W.; Jung, H. H.; Song, J.; Yang, C.; Wang, A.; Liu, Z.; Lee, J. Y.; Kim, B. H.; Kim, J.-H.; Lee, J.; Yu, Y.; Kim, B. J.; Jang, H.; Yu, K. J.; Kim, J.; Lee, J. W.; Jeong, J.-W.; Song, Y. M.; Huang, Y.; Zhang, Y.; Rogers, J. A. Self-Assembled Three Dimensional Network Designs for Soft Electronics. *Nat. Commun.* **2017**, *8*, 15894.

(6) Kim, H.; Kim, Y. S.; Mahmood, M.; Kwon, S.; Zavanelli, N.; Kim, H. S.; Rim, Y. S.; Epps, F.; Yeo, W. H. Fully Integrated, Stretchable, Wireless Skin-Conformal Bioelectronics for Continuous Stress Monitoring in Daily Life. *Adv. Sci.* **2020**, *7*, 2000810.

(7) Choi, J.; Kwon, D.; Kim, B.; Kang, K.; Gu, J.; Jo, J.; Na, K.; Ahn, J.; Del Orbe, D.; Kim, K.; Park, J.; Shim, J.; Lee, J.-Y.; Park, I. Wearable Self-Powered Pressure Sensor by Integration of Piezo-transmittance Microporous Elastomer with Organic Solar Cell. *Nano Energy* **2020**, *74*, 104749.

(8) Xu, S.; Zhang, Y.; Cho, J.; Lee, J.; Huang, X.; Jia, L.; Fan, J. A.; Su, Y.; Su, J.; Zhang, H.; Cheng, H.; Lu, B.; Yu, C.; Chuang, C.; Kim, T.-i.; Song, T.; Shigeta, K.; Kang, S.; Dagdeviren, C.; Petrov, I.; Braun, P. V.; Huang, Y.; Paik, U.; Rogers, J. A. Stretchable Batteries with Self-Similar Serpentine Interconnects and Integrated Wireless Recharging Systems. *Nat. Commun.* **2013**, *4*, 1543.

(9) Won, P.; Park, J. J.; Lee, T.; Ha, I.; Han, S.; Choi, M.; Lee, J.; Hong, S.; Cho, K.-J.; Ko, S. H. Stretchable and Transparent Kirigami Conductor of Nanowire Percolation Network for Electronic Skin Applications. *Nano Lett.* **2019**, *19*, 6087–6096.

(10) Brenneman, J.; Tansel, D. Z.; Fedder, G. K.; Panat, R. Interfacial Delamination and Delamination Mechanism Maps for 3D Printed Flexible Electrical Interconnects. *Extreme Mech. Lett.* **2021**, *43*, 101199.

(11) Jeong, Y. R.; Kim, J.; Xie, Z.; Xue, Y.; Won, S. M.; Lee, G.; Jin, S. W.; Hong, S. Y.; Feng, X.; Huang, Y.; Rogers, J. A.; Ha, J. S. A skin-Attachable, Stretchable Integrated System Based on Liquid GaInSn for Wireless Human Motion Monitoring with Multi-Site Sensing Capabilities. *NPG Asia Mater.* **2017**, *9*, No. e443.

(12) Kim, K.; Choi, J.; Jeong, Y.; Cho, I.; Kim, M.; Kim, S.; Oh, Y.; Park, I. Highly Sensitive and Wearable Liquid Metal-Based Pressure Sensor for Health Monitoring Applications: Integration of a 3D-Printed Microbump Array with the Microchannel. *Adv. Healthcare Mater.* **2019**, *8*, 1900978.

(13) Park, T. H.; Kim, J. H.; Seo, S. Facile and Rapid Method for Fabricating Liquid Metal Electrodes with Highly Precise Patterns via One-Step Coating. *Adv. Funct. Mater.* **2020**, *30*, 2003694.

(14) Kim, K.; Ahn, J.; Jeong, Y.; Choi, J.; Gul, O.; Park, I. All-Soft Multiaxial Force Sensor Based on Liquid Metal for Electronic Skin. *Micro Nano Syst. Lett.* **2021**, *9*, 2.

(15) Byun, J.; Oh, E.; Lee, B.; Kim, S.; Lee, S.; Hong, Y. A Single Droplet-Printed Double-Side Universal Soft Electronic Platform for Highly Integrated Stretchable Hybrid Electronics. *Adv. Funct. Mater.* **2017**, *27*, 1701912.

(16) Cao, Y.; Zhang, G.; Zhang, Y.; Yue, M.; Chen, Y.; Cai, S.; Xie, T.; Feng, X. Direct Fabrication of Stretchable Electronics on a Polymer Substrate with Process-Integrated Programmable Rigidity. *Adv. Funct. Mater.* **2018**, *28*, 1804604.

(17) Biswas, S.; Schoeberl, A.; Hao, Y.; Reiprich, J.; Stauden, T.; Pezoldt, J.; Jacobs, H. O. Integrated Multilayer Stretchable Printed Circuit Boards Paving the Way for Deformable Active Matrix. *Nat. Commun.* **2019**, *10*, 4909.

(18) Green Marques, D.; Alhais Lopes, P.; T. de Almeida, A.; Majidi, C.; Tavakoli, M. Reliable Interfaces for EGaIn Multi-Layer Stretchable Circuits and Microelectronics. *Lab Chip* **2019**, *19*, 897–906.

(19) Huang, Z.; Hao, Y.; Li, Y.; Hu, H.; Wang, C.; Nomoto, A.; Pan, T.; Gu, Y.; Chen, Y.; Zhang, T.; Li, W.; Lei, Y.; Kim, N.; Wang, C.; Zhang, L.; Ward, J. W.; Maralani, A.; Li, X.; Durstock, M. F.; Pisano, A.; Lin, Y.; Xu, S. Three-Dimensional Integrated Stretchable Electronics. *Nat. Electron.* **2018**, *1*, 473–480.

(20) Bartlett, M. D.; Markvicka, E. J.; Majidi, C. Rapid Fabrication of Soft, Multilayered Electronics for Wearable Biomonitoring. *Adv. Funct. Mater.* **2016**, *26*, 8496–8504.

(21) Cao, H. C.; Evans, A. G. An Experimental Study of the Fracture Resistance of Bimaterial Interfaces. *Mech. Mater.* **1989**, *7*, 295–304.

(22) Kok, C. M.; Yee, V. H. The Effects of Crosslink Density and Crosslink Type on the Tensile and Tear Strengths of NR, SBR and EPDM Gum Vulcanizates. *Eur. Polym. J.* **1986**, *22*, 341–345.

(23) Marletta, G. Chemical Reactions and Physical Property Modifications Induced by keV Ion Beam in polymers. *Nucl. Instrum. Methods Phys. Res., Sect. B* **1990**, *46*, 295–305.

(24) Wu, D.; Xu, F.; Sun, B.; Fu, R.; He, H.; Matyjaszewski, K. Design and Preparation of Porous Polymers. *Chem. Rev.* **2012**, *112*, 3959–4015.

(25) Kim, T.; Lee, H.; Jo, W.; Kim, T. S.; Yoo, S. Realizing Stretchable OLEDs: A Hybrid Platform Based on Rigid Island Arrays on a Stress-Relieving Bilayer Structure. *Adv. Mater. Interfaces* **2020**, *5*, 2000494.

(26) Kokkinis, D.; Bouville, F.; Studart, A. R. 3D Printing of Materials with Tunable Failure via Bioinspired Mechanical Gradients. *Adv. Mater.* **2018**, *30*, 1705808.

(27) Naserifar, N.; LeDuc, P. R.; Fedder, G. K. Material Gradients in Stretchable Substrates toward Integrated Electronic Functionality. *Adv. Mater.* **2016**, *28*, 3584–3591.

(28) Babu, S.; Lee, J. B. Plasma-Treated PDMS as Intrinsically Non Wetting Surface for Gallium-Alloy Liquid Metal Microfluidics. *The 33rd IEEE International Conference on Micro Electro Mechanical Systems (MEMS 2020)*: Vancouver, Canada, January 2020; pp 1122–1125.

(29) Jiang, Y.; Su, S.; Peng, H.; Sing Kwok, H.; Zhou, X.; Chen, S. Selective Wetting/Dewetting for Controllable Patterning of Liquid Metal Electrodes for All-Printed Device Application. *J. Mater. Chem. C* **2017**, *5*, 12378–12383.

(30) Ozutemiz, K. B.; Wissman, J.; Ozdoganlar, O. B.; Majidi, C. EGaIn-Metal Interfacing for Liquid Metal Circuitry and Microelectronics Integration. *Adv. Mater. Interfaces* **2018**, *5*, 1701596.

(31) Watson, A. M.; Cook, A. B.; Tabor, C. E. Electrowetting-Assisted Selective Printing of Liquid Metal. *Adv. Eng. Mater.* **2019**, *21*, 1900397.

(32) Tang, J.; Zhao, X.; Li, J.; Guo, R.; Zhou, Y.; Liu, J. Gallium-Based Liquid Metal Amalgams: Transitional-State Metallic Mixtures (TransM^{2}ixes) with Enhanced and Tunable Electrical, Thermal, and Mechanical Properties. *ACS Appl. Mater. Interfaces* **2017**, *9*, 35977–35987.

(33) Bark, H.; Lee, P. S. Surface Modification of Liquid Metal as an Effective Approach for Deformable Electronics and Energy Devices. *Chem. Sci.* **2021**, *12*, 2760–2777.

(34) Lin, W.; Qiu, W.; Tuersun, Y.; Huang, X.; Chu, S. Ultrastrong Spontaneous Surface Wetting of Room Temperature Liquid Metal on Treated Metal Surface. *Adv. Mater. Interfaces* **2021**, *8*, 2100819.

(35) Kim, S.; Amjadi, M.; Lee, T.-I.; Jeong, Y.; Kwon, D.; Kim, M. S.; Kim, K.; Kim, T.-S.; Oh, Y. S.; Park, I. Wearable, Ultrawide-Range, and Bending-Insensitive Pressure Sensor Based on Carbon Nanotube Network-Coated Porous Elastomer Sponges for Human Interface and Healthcare Devices. *ACS Appl. Mater. Interfaces* **2019**, *11*, 23639–23648.

(36) Lee, T.-I.; Jo, W.; Kim, W.; Kim, J.-H.; Paik, K.-W.; Kim, T.-S. Direct Visualization of Cross-Sectional Strain Distribution in Flexible Devices. *ACS Appl. Mater. Interfaces* **2019**, *11*, 13416−13422.

(37) Pan, B.; Qian, K.; Xie, H.; Asundi, A. Two-Dimensional Digital Image Correlation for In-Plane Displacement and Strain Measurement: a Review. *Meas. Sci. Technol.* **2009**, *20*, 062001.